Applied Catalysis B: Environmental 206 (2017) 490–500

Contents lists available at ScienceDirect

Applied Catalysis B: Environmental

journal homepage: www.elsevier.com/locate/apcatb

Mesoporous MFI zeolites as high performance catalysts for Diels-Alder cycloaddition of bio-derived dimethylfuran and ethylene to renewable *p*-xylene

Jeong-Chul Kim[a], Tae-Wan Kim[b,*], Youngjin Kim[a,c], Ryong Ryoo[a,d], Soon-Yong Jeong[b], Chul-Ung Kim[b]

[a] Center for Nanomaterials and Chemical Reactions, Institute for Basic Science (IBS), Daejeon 34141, Republic of Korea
[b] Center for Convergent Chemical Process, Korea Research Institute of Chemical Technology, 141 Gajeong-ro, Yuseong-gu, Daejeon 34114, Republic of Korea
[c] Department of Chemical and Biomolecular Engineering, KAIST, Daejeon 34141, Republic of Korea
[d] Department of Chemistry, KAIST, Daejeon 34141, Republic of Korea

ARTICLE INFO

Article history:
Received 14 October 2016
Received in revised form
15 December 2016
Accepted 12 January 2017
Available online 17 January 2017

Keywords:
MFI zeolite nanosheets
Hierarchical zeolite
p-Xylene production
Diels-Alder reaction

ABSTRACT

Zeolite solid-acid catalyst can produce *p*-xylene (PX) *via* a renewable synthetic route through Diels-Alder cycloaddition and dehydration reactions of bio-derived 2,5-dimethylfuran (DMF) and ethylene (DMF-to-PX). Here, to find a key factor in the physicochemical properties of a zeolite catalyst, we synthesized a series of mesoporous MFI zeolite nanosheets with systematically controlled thickness (2.5 and 7.5 nm) and silica-alumina ratio (Si/Al = 48–340) as well-defined model catalysts for PX production. From the catalytic results using these MFI zeolite nanosheets and conventional MFI zeolites, PX production yield was found to be strongly related to zeolite crystal thickness and concentration of Brønsted acid sites of the MFI zeolite catalysts. The MFI zeolite nanosheet with small thickness provided high PX production due to the presence of Brønsted acid sites on the exterior surface and facile mass transfer of aromatic compounds through mesopores. To verify these catalytic factors and to apply it to commercially available zeolite, a mesoporous MFI zeolite was prepared from a commercial ZSM-5 zeolite *via* a simple post-treatment process; mesoporous MFI-type zeolites were tested in the DMF-to-PX reaction. This mesoporous MFI zeolite exhibited a superior PX yield (75.8%) with high DMF conversion and PX selectivity compared with those characteristics of pristine MFI zeolite (PX yield = 8.4%).

1. Introduction

Isomeric xylenes (*ortho*-, *meta*- and *para*-xylene) have received much attention as valuable chemicals in the petrochemical industry [1,2]. During the last decade, the global consumption of xylenes has been increasing at a rate of 3.5% per year, this growth is expected to continue for the next five to ten years [3]. Among the three xylenes, *p*-xylene (PX) is the most important intermediate for the production of terephthalic acid and polyethylene terephthalate, which are in turn used for polymer production [2,4,5]. According to one market reports, over 26 billion tons of PX are produced globally per year [3]. PX is normally produced by catalytic cracking or steam reforming of crude oil feedstocks (*i.e.*, naphtha cracker) [6]. However, these petroleum-based processes have usually been operated with additional separation or purification treatments (*i.e.,* distillation, crystallization and adsorption) of the aromatic mixtures (*i.e.*, benzene, toluene and xylenes). On the other hand, PX can be synthesized directly through toluene (trans)alkylation, disproportionation and xylene isomerization reactions using a zeolite-based catalyst (*e.g.*, MFI zeolite) [6,7]. However, even these direct productions process have limitations due to the thermodynamic equilibrium of xylenes (20% *ortho*-, 55% *meta*- and 25% *para*-xylene) [8]. In addition, the production of aromatic feedstocks *via* petroleum-based process is expected to decrease with the latest shale gas exploration and development [9]. Some reports suggest that aromatic compounds from naphtha cracker are already down by 20% in the North America. At the same time, demand for aromatic compounds is expected to increase by 10% annually. Hence, these trends have brought about a great interest in the development of new technologies from bio-convertible and non-petroleum resources.

* Corresponding author.
E-mail address: twkim@krict.re.kr (T.-W. Kim).

http://dx.doi.org/10.1016/j.apcatb.2017.01.031
0926-3373/

Various alternative synthesis routes are being explored to produce PX from biomass-derived compounds. Biomass-based PX can be produced through aqueous-phase reforming and dehydrocyclization, fast pyrolysis and fermentation processes [10–12]. However, most of the processes studied to now seem to be in the early stages of research. Recently, new processes are being implemented to produce PX from bio-derived 2,5-dimethylfuran (DMF) with ethylene through Diels-Alder cycloaddition, followed by dehydration of the oxa-norbornene intermediate (DMF-to-PX route) [13]. Solid porous materials, such as zeolites, activated carbon, silica and alumina, are used as conventional catalysts in this biomass-based process. [14]. Among them, microporous zeolites have attracted considerable attention as solid acid catalysts due to their uniform microporosity, strong acidity, high stability and easy regenerability [5,15]. For example, zeolites with large pores (12-membered oxygen rings, 12-MR, *e.g.*, beta and USY) showed high PX production yield in the DMF-to-PX reaction, as compared with conventional porous solids. The high catalytic conversion of DMF and PX selectivity was due to confinement effects of the uniform micropores of the zeolite catalysts. However, even large pore zeolites still have small micropores, with pore diameters below 1 nm, resulting in molecular diffusion problems for reactants and products in the Diels-Alder cycloaddition reaction [5]. In a recent paper, our group reported for the first time that a mesoporous beta zeolite catalyst can be used as a high performance catalyst in the production of PX [16]. This result was explained by the unique hierarchical structure of the mesoporous beta zeolite catalyst.

As mentioned above, the beta zeolite catalyst is known as a high performance catalyst for the Diels-Alder cycloaddition reaction due to 12-MR large micropores [15]. Conventional bulk MFI zeolites are not as suitable as catalysts, because the 10-MR micropores are too small for the production of PX [5]. Recently, mesoporous MFI zeolite was reported by Ryoo and co-workers [17,18]. They developed a surfactant-directed zeolite synthesis method to mesoporous MFI zeolite using a di-quaternary ammonium-type surfactant as a structure-directing agent (SDA). In this synthesis route, MFI zeolite with a nanosheet-like morphology was synthesized by use of CH_3-$(CH_2)_{21}$–$N^+(CH_3)_2$–$(CH_2)_6$–$N^+(CH_3)_2$–$(CH_2)_5$–$CH_3(Br^-)_2$. The nanosheets MFI zeolite was composed of a disordered assembly of MFI nanocrystals that exhibited a sharp distribution of mesopore diameters centered at ~6 nm. It was possible to tailor the thickness of the MFI zeolite nanolayers in a range from 2.5 to 7.5 nm by changing the number of ammonium groups in the surfactants [19,20]. In addition, it was easy to obtain the nanosheets MFI zeolite in a wide range of Si/Al ratios (40-pure silica) [21]. The tunable acid sites of nanosheets MFI zeolite were found to be suitable for various catalytic reactions requiring strong acidity. For example, the nanosheets MFI zeolite exhibited high catalytic activity and product selectivity in the gas-phase methanol to hydrocarbon reaction, Friedel-Crafts reactions, and Pechmann condensation of large aromatic reactants in liquid-phase [21–26]. These results disclosed that the nanosheets MFI zeolite had a high concentration of strong Brønsted acid sites located on the mesopore wall. In addition, the systematically tunable physicochemical properties of MFI zeolite nanosheet, due to their structural uniformity (*e.g.* sheet thickness and pore size distribution), make this a model catalyst that can be used to find the key factor in the catalytic reaction with controllable acidity. The model mesoporous MFI zeolite nanosheet can be investigated by several measurement techniques such as electron microscopy analysis, gas adsorption-desorption, powder X-ray diffraction, and so on.

Herein, the Diels-Alder cycloaddition of DMF with ethylene was investigated over nanosheets MFI zeolites with different crystal sizes (2.5 and 7.5 nm) and Si/Al ratios (48, 78, 95, 155, 247, and 340). These results are discussed to find predominant reaction factors in DMF-to-PX reaction compared with the catalytic performance of MFI-type zeolite with various crystal thicknesses ranging from 500 to 2.5 nm. In order to verify the main factors and to apply this process to a commercial zeolite, a commercially available MFI-type zeolite (ZSM-5) was converted to a mesoporous MFI zeolite by a simple post-treatment; the material was then tested in the DMF-to-PX reaction.

2. Experiment

2.1. Material synthesis

Nanosheets MFI-type zeolite samples with two types of thicknesses were synthesized *via* surfactant-directed hydrothermal synthesis method, as described elsewhere [21]. The 2.5 nm thick nanosheets MFI zeolite was synthesized using di-quaternary ammonium containing surfactants $[CH_3$-$(CH_2)_{21}$–$N^+(CH_3)_2$–$(CH_2)_6$–$N^+(CH_3)_2$–$(CH_2)_5$–$CH_3(Br^-)_2$, in short, $C_{22\text{-}6}N_2(Br)_2]$ as an structure-directing (SD) surfactant. The Si/Al ratios of nanosheets MFI zeolite was varied in the range of 50–350. The molar gel compositions were 7.5 $C_{22\text{-}6}N_2(Br)_2$:*n* Al_2O_3:100 SiO_2:4000 H_2O:24 H_2SO_4:30 Na_2O, where *n* is ranging from 0.142 to 1. For the nanosheets MFI zeolite with 7.5 nm thickness, the zeolite was synthesized using multi-quaternary ammonium containing surfactant $\{CH_3$-$(CH_2)_{21}$–$N^+(CH_3)_2$–$[(CH_2)_6$–$N^+(CH_3)_2]_3$–$(CH_2)_5$–$CH_3(Br^-)_4$, in short, $C_{22\text{-}6}N_4(Br)_4\}$. The gel composition was 2.5 $C_{22\text{-}6}N_4(Br)_4$:0.1 Al_2O_3:100 SiO_2:4000 H_2O:20 H_2SO_4:30 Na_2O. The synthesis conditions for nanosheets MFI zeolite samples were the same as described by Kim et al. [21]. These zeolite samples are denoted as "NS-*x*-(*y*)", according to the crystal thickness (*x* = 2.5 and 7.5) and Si/Al ratio (*y* = 48, 78, 95, 155, 247, and 340) determined by the transmission electron microscopy and the elemental analysis.

The bulk crystalline MFI was also prepared *via* hydrothermal synthesis route using tetrapropylammonium hydroxide (TPAOH). The synthesis details are described elsewhere [22]. This zeolite is designated as "B-500", meaning "500 nm thick bulk MFI zeolite". All synthesized zeolite samples (both nanosheets and bulk zeolite) were calcined at 823 K to remove the SD surfactant. In order to prepare acidic- zeolite, the calcined samples were slurried in a 1.0 M NH_4NO_3 aqueous solution three times, followed by calcination in air at 823 K. A commercial zeolite with MFI structure (type material: ZSM-5, CBV 8014, Si/Al = 42) was provided from Zeolyst International. This sample is denoted as "C-60", according to the mean crystal thickness.

Three additional mesoporous ZSM-5 zeolites were prepared in our lab from a commercially available ZSM-5 (denoted as "Pristine ZSM-5", Zeolyst International, CBV 2314, Si/Al = 11.5) by a NaOH desilication and a modified pseudomorphic synthesis [27]. The first method, NaOH desilication, is as follows: the commercial ZSM-5 (2.0 g) was mixed with 0.2 M NaOH aqueous solution (15 ml), and the mixture solution was stirred at 343 K for 4 h. The NaOH-treated sample was recovered by centrifugation and extensive washing with DI water and was dried for 6 h at 373 K. Lastly, the sodium form zeolite sample was converted into acidic zeolite by ion-exchange (3 times) with an ammonium nitrate aqueous solution (1.0 M) and calcination processes. The resultant NaOH treated sample is denoted as "Meso-ZSM-5-NaOH". Two mesoporous ZSM-5 samples were synthesized from the commercial ZSM-5 *via* pseudomorphic synthesis with different molar ratios of trimethylammonium hydroxide (TMAOH):hexadecyltrimethylammonium bromide (CTAB) = 2 and 3. Briefly, the commercial H-ZSM-5 zeolite (1.67 g) and 0.83 g of CTAB (VWR Co.) were added to 50 ml of 0.09 M and 0.135 M TMAOH (Sigma-Aldrich, 25 wt% in water) for CTAB:TMAOH = 2 and 3, respectively. After stirring at room temperature for 30 min, the synthesis gel was hydrothermally treated in a

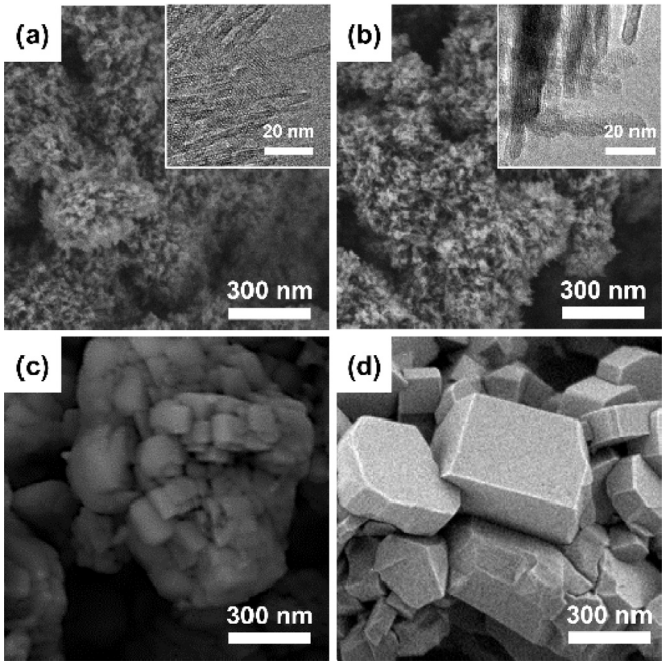

Fig. 1. Representative SEM and TEM images of (a) NS-2.5, (b) NS-7.5, (c) C-60, and (d) B-500 samples.

Teflon-lined autoclave for 20 h at 423 K. After hydrothermal treatment, the resultant zeolite was filtered and extensively washed with DI water. The zeolite was dried for 6 h at 348 K and calcined under air flow at 823 K. These samples are designated as "Meso-ZSM-5-2" and "Meso-ZSM-5-3", where "2" and "3" stand for the CTAB:TMAOH molar ratios.

2.2. Characterization

High-resolution scanning electron microscopy (SEM) images were obtained without a metal coating, operating a FEI Verios^{TM} 460L with a 0.5 kV operating voltage in deceleration mode (4 kV). High-resolution TEM images were taken by using an FEI Titan^{TM} ETEM G^2 with an acceleration voltage of 300 kV. A Rigaku Multiplex instrument diffractometer (40 mA, 30 kV, Cu Kα radiation) measured X-ray diffraction (XRD) patterns of the samples. N_2 physorption isotherms were analyzed at liquid N_2 temperature (77 K) using a Tristar II (Micromeritics) after sample outgassing at 573 K for 6 h. The elemental composition analysis was measured by inductively-coupled plasma atomic emission spectroscopy (ICP-AES, OPTIMA 4300 DV, Perkin Elmer). In order to characterize Brønsted acid properties (locations and concentrations), ^{31}P NMR spectra were recorded on a Bruker AVANCE 400 WB, following a procedure based on previously reported method [28,29].

2.3. Catalytic reactions

The Diels-Alder cycloaddition reaction was performed at 523 K in a high-pressure batch reactor system. Typically, 0.2 g of MFI zeolite catalyst was added to the batch-type reactor that contained 25 ml of 2,5-dimethylfuran (Acros, 99%) and 75 ml of *n*-heptane (J. T. Baker, 99%). Prior to the catalytic reaction, the purging was carried out in a reactor vessel by high-purity N_2 gas to prevent contamination by air, moisture and impurities. After purging the reactor with N_2 gas, ethylene (purity 99.5%) was introduced into the vessel. The reactor was then pressurized to 50 bar with ethylene. During the reaction time, the constant pressure of the reactor vessel was maintained by supplying ethylene gas. The reactor was equipped with a mechanical stirring system (500 rpm) and heated to the target reaction temperature (523 K). Using a double block sampling system, small aliquots (0.5 ml) of the samples were taken from the vessel at different reaction times afterward. The collected liquid product was analyzed by a gas chromatograph with a flame ionization detector and an HP-INNOWAX column (0.32 mm id × 0.5 μm thickness × 60 m length).

2.4. Recycle test

The recyclability of the NS-2.5 catalyst was investigated in the DMF-to-PX reaction. After 1st reaction cycle for 8 h, the used NS-2.5 catalyst was collected from the reaction mixture by centrifugation. Before the 2nd catalytic cycle, the collected NS-2.5 sample was washed with *i*-propyl alcohol several times and then dried overnight at 373 K. The 2nd cycle was performed over the dried NS-2.5 sample without further treatment. For the reaction cycles (3rd–6th), the dried NS-2.5 sample was calcined for 4 h at 823 K under air flow to remove the organic deposit. In the case of the 7th cycle, the catalytic activity was measured over the calcined NS-2.5 catalyst under same reaction condition, except for 24 h of reaction time.

3. Results and discussion

3.1. Properties of MFI nanosheet and MFI-type zeolite catalysts

TEM and SEM images of a series of MFI-type zeolites were shown in Fig. 1. NS-2.5 was synthesized using a $C_{22\text{-}6}N_2(Br)_2$ structure-directing surfactant. The NS-2.5 sample exhibited a nanosheet-like morphology, composed of zeolitic nanolayers of 2.5 nm thickness with high crystallinity. The MFI nanosheets were randomly interconnected each other to form a disordered network structure, as reported previously [30]. The NS-7.5 was obtained using same synthesis condition, except that the $C_{22\text{-}6}N_4(Br)_4$ surfactant was used as SDA in this case. The NS-7.5 showed a crystal morphology very similar to that of the NS-2.5 sample; it consisted of MFI nanolayers with 7.5 nm thickness along the crystal *b*-axis. C-60 displayed the gathering of primary MFI zeolite particles with a broad distribution in a diameter range of 60 to 100 nm. B-500 was synthesized with TPAOH in the form of a bulk crystal-like particle morphology with smooth facets. The diameters of the bulk zeolite crystals ranged from 500 nm to 1 μm. No significant presence of any amorphous impurities was observed in the all MFI zeolite samples upon SEM, TEM and XRD investigations.

The XRD patterns of the MFI zeolite samples are shown in Fig. 2(a). All MFI zeolite samples showed Bragg reflection lines in the wide angle region diffraction patterns, which were characteristics of highly crystalline MFI-type zeolite structure. No background increase attributable to non-crystalline silicates was detected in the 2θ range of 15–25°. The peak intensities decreased with a decreasing zeolite crystallite thickness while the XRD line widths were found to change in an inverse fashion. In particular, the XRD patterns of two types of nanosheets MFI zeolite samples (NS-2.5 and NS-7.5) showed noticeable peak broadening and (*h0l*) predominant reflections due to a loss of long-range order along the *b*-axis. This result could be attributed to the spatial restriction of crystal growth along a specific direction, such as *b*-axis, by the hydrophobic parts of the structure-directing surfactants. This is in good agreement with the ultrathin crystal thickness in the nanosheets MFI zeolite confirmed by TEM investigation. No other Bragg reflections were identified in the XRD patterns due to their peak broadening and low intensities.

The porous properties of the MFI zeolite samples were evaluated by the nitrogen sorption isotherms shown in Fig. 2(b). The physic-

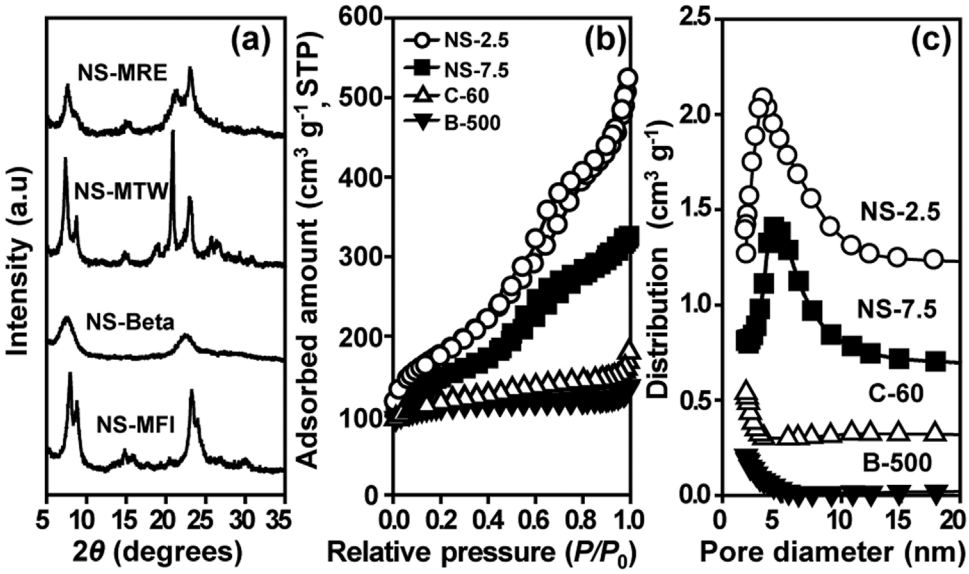

Fig. 2. Powder XRD patterns (a), nitrogen sorption isotherms (b), and pore size distribution corresponding to the adsorption branch (c) of NS-2.5, NS-7.5, C-60, and B-500.

Table 1
Physicochemical properties of NS-2.5, NS-7.5, C-60, and B-500 samples.

Catalyst	Si/Al[a]	S_{BET} ($m^2\ g^{-1}$)[b]	S_{ext} ($m^2\ g^{-1}$)[c]	V_{tot} ($cm^3\ g^{-1}$)[d]	BA_{tot} ($\mu mol\ g^{-1}$)[e]	BA_{ext} ($\mu mol\ g^{-1}$)[f]
NS-2.5	48	620	460	0.73	162	49
NS-7.5	47	520	310	0.50	164	43
C-60	42	360	40	0.18	178	21
B-500	50	300	20	0.15	158	4

[a] Si/Al molar ratio obtained from ICP-AES elemental analysis.
[b] S_{BET} is the BET surface area obtained from N_2 adsorption in relative pressure range (P/P_0) of 0.05–0.20.
[c] S_{ext} is the external surface area evaluated from the *t*-plot method.
[d] V_{tot} is the total pore volume obtained at $P/P_0 = 0.95$.
[e] BA_{tot} is the concentration of total Brønsted acid sites.
[f] BA_{ext} is the concentration of external Brønsted acid sites.

ochemical properties of all investigated MFI zeolite samples are displayed in Table 1. The N_2 sorption isotherms of the NS-2.5 sample displayed characteristic type IV isotherms with a steep capillary condensation in the range of relative pressure (P/P_0) from 0.4 to 0.5, which is due to the well-known capillary condensation in intercrystalline mesopores between zeolite nanosheets. The hysteresis loop of the NS-2.5 sample was of type H2 form, which indicates ink-bottle shaped pores. This result is a distinctive feature of the disordered mesoporous materials [31]. The BJH algorithm was used to determine the size of the mesopores. As can be seen in Fig. 3(c), the obtained mesopore size distribution exhibited a narrow peak centered at 6 nm, with high total pore volume (0.73 $cm^3\ g^{-1}$). These mesoporous properties of the NS-2.5 sample is comparable with those of the amorphous MCM-41-type silicas [32]. The NS-2.5 sample possesses high specific surface area (620 $m^2\ g^{-1}$) and external surface area (460 $m^2\ g^{-1}$), as determined by the BET equation and the *t*-plot method, respectively. For the NS-7.5 sample, the adsorption isotherm was similar to that of NS-2.5, except for the type H3 hysteresis loop, which is associated with slit-typed mesopores. In the case of the C-60 and B-500 samples, the adsorption isotherm was of a type I isotherm, which indicates solely microporous zeolites. Hence, these two samples have very low external surface area, as compared with nanosheets MFI zeolite samples. These observed results are in good agreement with XRD and TEM investigation given above.

Table 1 shows Si/Al ratios of the investigated MFI zeolite catalysts, based on the results of ICP-AES spectroscopy. All MFI zeolite samples possessed similar Si/Al ratios of 42–50 but differed in Brønsted acidic properties. The concentration and location of the

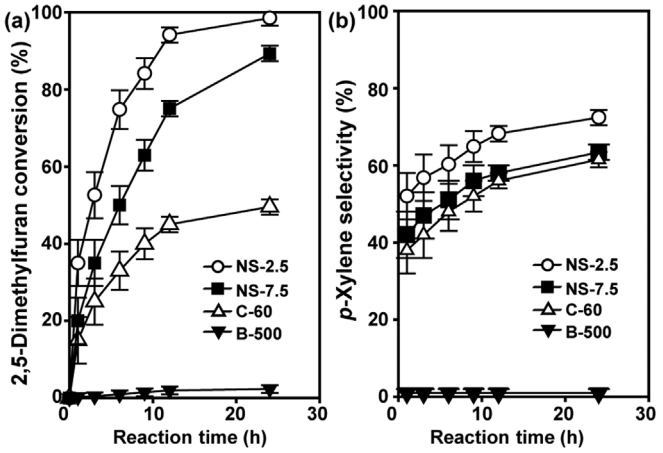

Fig. 3. Conversion of 2,5-dimethylfuran (a) and *p*-xylene selectivity (b) over NS-2.5, NS-7.5, C-60, and B-500 catalysts as a function of reaction time. Reaction conditions: 0.2 g of catalyst, 25 ml of 2,5-dimethylfuran, 50 bar of ethylene, 75 ml of *n*-heptane (solvent), 523 K.

Brønsted acid sites in all the MFI zeolite samples were characterized by ^{31}P NMR analysis using phosphine oxides containing molecules as probe titrants. Brønsted acid sites of the entire zeolite crystals (BA_{tot}) were calculated using trimethylphosphine oxide (TMPO). TMPO (kinetic diameter = 0.5 nm) can adsorb the Brønsted acid sites inside micropores (10-MR, 0.51 × 0.55 and 0.53 × 0.55 nm) as well as on the exterior surface of the MFI zeolite. All MFI zeolite

Table 2
2,5-Dimethylfuran conversion and product selectivity of NS-2.5, NS-7.5, C-60, and B-500 catalysts for the DMF-to-PX reaction at 24 h of reaction time.

Catalyst	H-TOF (10^{-3} s^{-1})[a]	DMF Conv. (%)	NPA ($\times 10^{-3}$)[b]	PX yield (%)	Selectivity (%)[c]			
					PX	MX	HDO	Unknown products
NS-2.5	184.4	95.8	6.8	69.8	72.4	1.4	6.3	19.9
NS-7.5	84.1	89.4	6.1	56.7	63.5	0.1	10.9	25.5
C-60	52.6	49.7	3.2	30.5	61.5	0.7	9.5	28.3
B-500	0.01	2.3	0.1	–	–	–	12.7	87.3

[a] H-TOF is the turnover frequency calculated by normalizing the rate by the number of Brønsted acid sites at the reaction time = 1 h.
[b] NPA is number of molecules per acids site calculated by the mole of reacted DMF by the number of Brønsted acid sites in the catalyst.
[c] MX, *m*-xylene; HDO, 2,5-hexanedione; Unknown products, carbon loss.

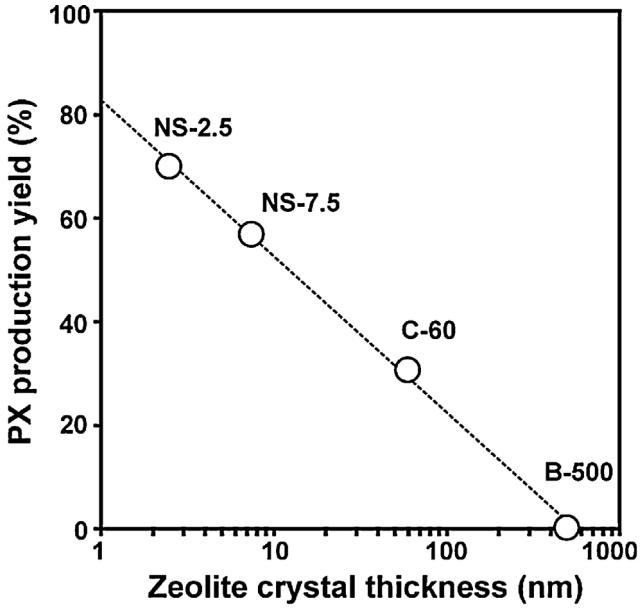

Fig. 4. Plot for zeolite crystal thickness *versus* PX production yield of NS-2.5, NS-7.5, C-60 and B-500 catalysts. Reaction conditions: 0.2 g of catalyst, 25 ml of 2,5-dimethylfuran, 50 bar of ethylene, 75 ml of *n*-heptane (solvent), 523 K, 24 h.

samples possessed a similar number of BA_{tot} (158–178 μmol g^{-1}). In addition, Brønsted acid sites on the exterior surface of the MFI zeolite (BA_{ext}) were detected using tributylphosphine oxide (TBPO, 0.82 nm). The value of BA_{ext} increased in the order of B-500 (4 μmol g^{-1}) < C-60 (21) < NS-7.5 (43) < NS-2.5 (49). These results are due to the presence of open mesopores of the nanosheets MFI samples. From these results, it was concluded that NS-2.5 contained 30% of Brønsted acids on the exterior surface of these zeolite crystals, whereas were only 3% of the accessible Brønsted acids on the external surface for B-500. In addition, the strong Brønsted acid sites of all MFI zeolite samples could be calculated from the peak deconvolution of ^{31}P MAS NMR spectra using a Gaussian method (corresponding to the chemical shift of 86 and 92 ppm in ^{31}P MAS NMR spectra of TMPO and TBPO, respectively). The concentration and location of the strong Brønsted acid sites are shown in Table S1. All MFI zeolite samples had a similar amount of strong BA_{tot} (11–14 μmol g^{-1}), which were located both on the external surface and inside the micropores. Among them, the strong BA_{ext} increased with decreasing crystal thickness. In particular, the NS-2.5 sample possessed highest amount of strong BA_{ext} (10 μmol g^{-1}, strong BA_{ext}/BA_{tot} = 71%), among all investigated MFI zeolite samples. In the case of B-500 sample, strong Brønsted acid sites mainly located inside micropores of large zeolite crystals (0.5 μmol g^{-1}, strong BA_{ext}/BA_{tot} = 4.5%). This result is similar to results with of MFI zeolite nanosheets synthesized *via* the same synthesis approach, as shown in a previous report [28].

3.2. Catalytic performance of DMF-to-PX over nanosheets MFI zeolites and MFI-type zeolite with different wall thicknesses

The catalytic properties of all MFI zeolite samples were investigated in PX production from DMF and ethylene though Diels-Alder cycloaddition reaction. The catalytic performance is evaluated by focusing on the catalytic DMF conversion and PX selectivity at 523 K and 50 bar. The DMF conversion and PX selectivity are plotted against reaction times in Fig. 3. The plot shows that the DMF conversion over all MFI zeolite catalysts increased within 1 h of reaction time. The initial DMF conversion rate increased in the following order: B–500 < C–60 < NS-7.5 < NS-2.5. The B-500 catalyst showed a negligible catalytic conversion of DMF and PX selectivity. This low catalytic conversion is explained by diffusion limitation of reactant and product molecules inside micropores of the MFI zeolite catalyst (0.51 × 0.55 and 0.53 × 0.55 nm). Both the reactant (DMF, kinetic diameter = 0.57 nm) and major product (PX, 0.58 nm) were too bulky to penetrate into the MFI zeolite micropores with large crystal thickness. However due to its highly mesoporous texture (*i.e.*, high external surface area and large pore volume), the NS-2.5 catalyst exhibited much higher catalytic conversion at the early period than that of the B-500 catalyst, resulting in the rapid molecular diffusion through mesopores. From this result, the turnover frequencies (H-TOF) for the production of PX with MFI zeolite catalysts were calculated by normalizing the rate by the number of Brønsted acid sites as determined by ^{31}P NMR spectroscopy of adsorbed TMPO (shown in Table 1). The H-TOF increased in the order of B-500 (0.01) < C-60 (52.6) < NS-7.5 (84.1) < NS-2.5 (184.4).

At this time, the NS-2.5 catalyst showed high selectivity (~60%) to PX. The PX was quickly produced *via* Diels-Alder cycloaddition, followed dehydration processes of DMF with ethylene over the NS-2.5 catalyst. The high selectivity to PX was attributed to the high density of Brønsted acid sites placed on the exterior surface of the NS-2.5 catalyst. This is consistent with a previous report on the high catalytic conversion rate of nanosponge beta zeolite due to mesoporous structures and catalytically active sites existing on the external surface of beta zeolite crystallites in the Diels-Alder cycloaddition reaction [16]. In order to investigate the effect of mesoporosity of zeolite catalyst on catalytic performance in the PX production, additional catalytic reaction was performed over microporous Beta zeolite (Zeolyst, CBV814E, Si/Al = 12.5) under same reaction condition (Fig. S1). The Beta zeolite exhibited similar DMF conversion to the NS-2.5 catalyst. However, there was a remarkable difference in the PX selectivity (56% with NS-2.5 and 15% with Beta zeolite) at the initial stage of the reaction. This result indicated that PX selectivity could be enhanced by the generation of mesopores in the zeolite catalyst due to facile diffusion of molecules.

After the initial reaction stage, DMF conversion over all the MFI zeolite catalysts gradually increased to the maximum conversion value at about 24 h. The DMF conversion and product selectivity of all investigated zeolite catalysts are shown in Table 2. The order

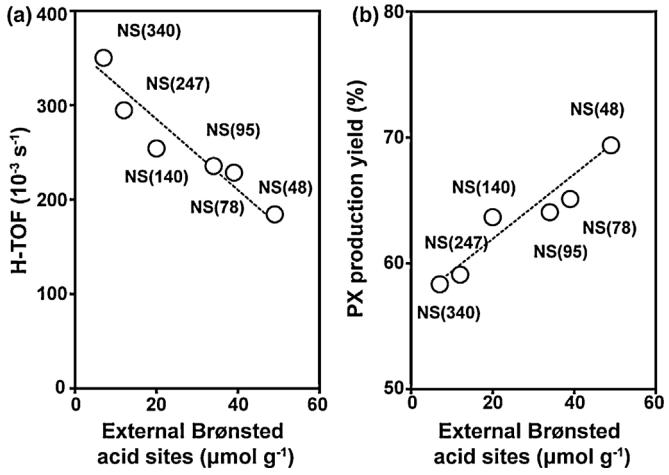

Fig. 5. Plot for external Brønsted acid sites *versus* H-TOF (a) and PX production yield (b) of NS-2.5-(*x*) (*x* = 48, 78, 95, 140, 247, and 340) catalysts. Reaction conditions: 0.2 g of catalyst, 25 ml of 2,5-dimethylfuran, 50 bar of ethylene, 75 ml of *n*-heptane (solvent), 523 K, 24 h.

of the maximum values at 24 h among these catalysts was NS-2.5 (95.8%) > NS-7.5 (89.4%) > C-60 (49.7%) > B-500 (2.3%), according to the crystal thickness of the MFI zeolite samples. From this result, the reaction rate was calculated from the DMF conversion by the number of converted reactants per active site for 24 h of reaction time, based on the sum total of Brønsted acid sites as achieved by the ^{31}P NMR analysis (Table 1). This total number is designated as "NPA", where NPA denotes 'number of converted reactants per Brønsted acid site' of the MFI zeolite catalyst. Table 2 shows the NPA values of all the investigated catalysts in the DMF-to-PX at 523 K. The following order of NPA values in the DMF-to-PX reaction was derived: B-500 (0.1) < C-60 (3.2) < NS-7.5 (6.1) < NS-2.5 (6.8). In particular, the NPA value calculated for the two nanosheets MFI zeolite catalysts (NS-2.5 and NS-7.5) are similar to each other compared with conventional MFI zeolite catalysts (C-60 and B-500). This similarity may be due to the effect of active functions in the zeolite morphologies (surface fractality, roughness, defect sites, and aluminum distribution) promoting Diels-Alder cycloaddition reaction over the nanosheets MFI zeolite catalysts. The difference in catalytic activity of the nanosheets MFI zeolites may be connected with the different mesoporosity of nanosheets MFI zeolite catalysts [25,33]. In contrast to the nanosheets MFI zeolites, the low values of NPA calculated for C-60 and B-500 may indicate the catalytic deactivation of C-60 and B-500 catalysts during the reaction time.

The PX yield of all the MFI zeolite catalysts is shown in Table 2. The PX yield increased in the order of B-500 (0%) < C-60 (30.5%) < NS-7.5 (56.7%) < NS-2.5 (69.8%) in the PX production reaction at 24 h of reaction time. Notably, a correlation was observed between the PX yield and the crystal thickness of MFI zeolite catalysts, as shown in Fig. 4. The resulting correlation shows that the PX yield increased in a linear manner with decreasing MFI zeolite crystal thickness. This trend can be explained by the formation of by-products (2,5-hexanedione and unknown products) *via* side reaction routes such as DMF hydrolysis with water in the conventional MFI zeolite with large crystal thickness (C-60 and B-500). These by-products can be easily changed into polymeric coke precursors by strong Brønsted acid sites inside the micropores, and can block the access of reactants (DMF and ethylene) and cycloadduct intermediate molecules into the active sites. The amount of coke deposition for NS-2.5 and B-500 catalysts was measured by TGA analysis after 24 h of reaction time. As shown in Table S2, the spent NS-2.5 and B-500 catalysts possessed a similar amount of coke deposition in the DMF-to-PX reaction (NS-2.5 = 14.6 wt% and B–500 = 15.3 wt%, respectively), although there was a big difference in the DMF conversion at 24 h of reaction time (NS-2.5 = 95.8% and B–500 = 2.3%, respectively). This result indicates that the NS-2.5 sample is more coke-tolerable than B-500 sample. Thus, the B-500 catalyst was rapidly deactivated during the reaction. In addition, the low PX yield of C-60 and B-500 can be attributed to the low accessibility of reactant molecules to the catalytic active sites in the MFI zeolite catalysts with large crystal thickness. The MFI zeolite with thicker crystals (C-60 and B-500) showed low PX yield in the DMF-to-PX reaction due to the small amount of Brønsted acid sites on the external surface, as shown in Table 1. However, the PX yield could be increased up to 70% due to the generation of mesopores in the MFI zeolite catalyst (NS-2.5). This is a phenomenon commonly observed in various catalytic reactions involving bulky molecules that are difficult to enter zeolite micropores [25,26]. Such phenomenon can be attributed to the easy diffusion of molecules in the NS-2.5 catalyst. Therefore, the conventional MFI zeolite cannot be used as a catalyst in the DMF-to-PX reaction. However, the NS-2.5 catalyst, due to mesoporous structure, exhibited high catalytic DMF conversion and PX selectivity in the PX production reaction.

3.3. *Effect of the MFI zeolite nanosheets with different of Si/Al ratios on the catalytic performance of DMF-to-PX*

We performed an additional DMF-to-PX reaction under same reaction condition over NS-2.5 catalysts with different Si/Al ratios ranging from 48 to 340 to investigate the catalytic property of nanosheets MFI zeolite catalyst in more detail. In the present study, these samples were prepared, following the synthesis procedure described above [21]. Characterization of the nanosheets MFI samples using TEM (not shown), XRD and N_2 sorption analysis revealed that all nanosheets zeolite samples were prepared in the form of a three-dimensional disordered assembly of a 2.5-nm-thick MFI zeolite framework. The mesoporous textures of the synthesized nanosheets zeolite samples were very similar to that of NS-2.5. These samples had high specific BET surface areas and large total pore volumes (Fig. S2 and Table S3). The pore size distributions sharply peaked at 6 nm, as in the case of NS-2.5. Elemental analysis and ^{31}P NMR analysis were also performed for these samples, as was done for all investigated MFI zeolites. The results indicated that these samples contained high concentrations of strong Brønsted acid sites placed on the exterior surface in nanosheets MFI-type zeolite catalysts; this was also true of the NS-2.5 sample (Table S3). Based on these results, it can be concluded that nanosheets MFI zeolite samples with different Si/Al ratios possess comparable physicochemical properties, except for the total amount of Brønsted acidity in the zeolite catalysts.

Catalytic results of the NS-2.5-(*x*) samples (*x* = 48, 78, 95, 140, 247, and 340) for the DMF-to-PX reaction was shown in Fig. 5 and Table 3. All nanosheets MFI catalysts exhibited very similar catalytic DMF conversions (90–95%) with high PX selectivity (60–70%). This high selectivity to PX is due to the unique mesoporous properties as well as to the Brønsted acid sites of these nanosheets MFI catalysts. However, these samples displayed notable differences in H-TOF and NPA values. These values increased in the order of NS-2.5-(48) < NS-2.5-(78) < NS-2.5-(95) < NS-2.5-(140) < NS-2.5-(247) < NS-2.5-(340). In particular, the NS-2.5-(340) catalyst showed the highest H-TOF and NPA values (H-TOF = 350.2, NPA = 70.7) among all investigated MFI zeolite catalysts. As shown above, NS-2.5-(340) possessed the lowest number of Brønsted acid sites in the nanosheets surface (Table S3). Despite this low concentration of acidic sites, individual catalytic sites in NS-2.5-(340) were sufficiently strong, and these sites were active for the Diels-Alder cycloaddition and dehydration reaction. According to the overall reaction pathway described in the previous literature (as shown in Fig. S3) [5], the DMF-

Table 3
2,5-Dimethylfuran conversion and product selectivity of NS-2.5-(*x*) samples (*x* = 48, 78, 95, 140, 247, and 340) catalysts for the DMF-to-PX reaction at 24 h of reaction time.

Catalyst	H-TOF (10^{-3} s^{-1})[a]	DMF Conv (%)	NPA ($\times 10^{-3}$)[b]	PX Yield (%)	Selectivity (%)[c]			
					PX	MX	HDO	Unknown Products
NS-2.5-(48)	184.4	95.8	6.8	69.8	72.4	1.4	6.3	19.9
NS-2.5-(78)	228.4	95.6	9.6	65.1	69.0	1.3	8.1	21.6
NS-2.5-(95)	235.5	94.2	11.7	64.1	68.0	1.6	10.0	20.4
NS-2.5-(140)	254.1	95.3	14.7	63.7	66.8	1.1	10.2	21.9
NS-2.5-(247)	294.6	93.8	27.8	58.9	63.0	0.6	10.4	26.0
NS-2.5-(340)	350.2	91.7	70.7	58.4	63.6	0.8	11.2	24.4

[a] H-TOF is the turnover frequency calculated by normalizing the rate by the number of Brønsted acid sites at the reaction time = 1 h.
[b] NPA is number of molecules per acids site is calculated by the mole of reacted DMF by the number of Brønsted acid sites in the catalyst.
[c] MX, *m*-xylene; HDO, 2,5-hexanedione; Unknown products, carbon loss.

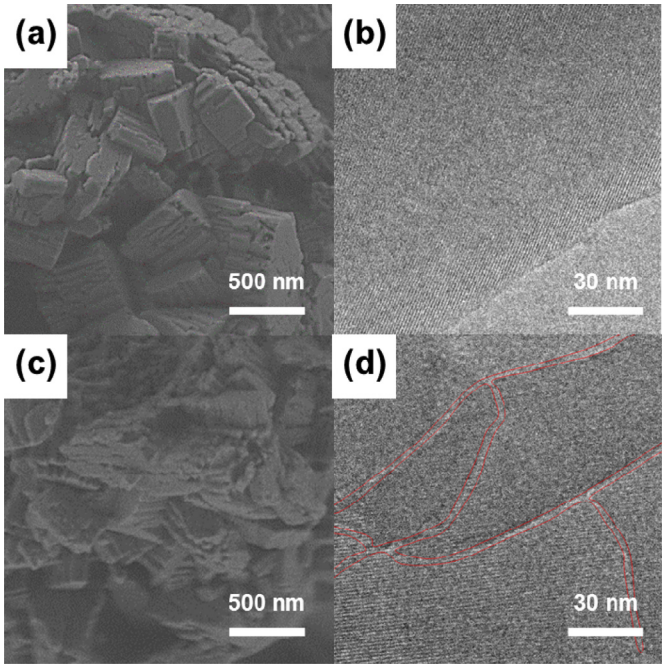

Fig. 6. Representative SEM and TEM images of pristine ZSM-5 [(a), (b)] and Meso-ZSM-5-3 sample [(c), (d)].

to-PX reaction proceeds through a two-step reaction. The first reaction step produces an oxa-norbornene cycloadduct intermediate in the Diels-Alder cycloaddition of DMF with ethylene. This reaction has been catalyzed by both Lewis and Brønsted acidic functions (*e.g.*, alumina, silica-alumina, and zeolite). On the other hand, the second step is thought to occur by dehydrative aromatization of cycloadduct intermediate. The dehydration reaction can be effectively promoted by the Brønsted acid sites of zeolite catalysts due to low energy barrier confirmed by DFT study [34]. Therefore, the Brønsted acid functions were an important factor affecting the PX production. In addition, mesoporous structure of the nanosheets MFI catalyst may result in high H-TOF and NPA values in the DMF-to-PX reaction. Compared to the NS-2.5-(140) catalyst (H-TOF = 254.1, NPA = 14.7), the C-60-(140) catalyst (Zeolyst, CBV 28014, Si/Al = 140) exhibited a low H-TOF and NPA values (66.6 and 5.6, respectively) due to low accessibility and diffusion limitations of the reactants and products (Tables S4 and S5). Thus, both the acidic properties (concentration, strength, and location) and morphologies of the zeolite catalyst may be a key factor in improving the catalytic activity in the DMF-to-PX reaction.

A plot of the PX production yield *versus* the number of Brønsted acid sites of the NS-2.5-(*x*) (*x* = 48, 78, 95, 140, 247, and 340) catalysts is shown in Fig. 5(b). The plot shows that the PX yield increased

Table 4
Recyclability test of NS-2.5 in the DMF-to-PX reaction of 2,5-dimethylfuran with ethylene.

Cycle	Conversion (%)	Selectivity (%)
1[a]	74.2	60.2
2[b]	29.6	51.0
3[c]	73.5	61.0
4[c]	73.2	60.8
5[c]	72.8	61.3
6[c]	72.5	60.1
7[d]	93.1	71.5

[a] Reaction conditions: 0.2 g of catalyst, 25 ml of 2,5-dimethylfuran, 50 bar of ethylene, 75 ml of *n*-heptane (solvent), 523 K, 8 h.
[b] For the 2nd cycle, the reaction was performed over the used catalyst after washing with *i*-propyl alcohol and drying at 373 K.
[c] The reaction cycles from 3rd to 6th were carried out with the catalyst after calcination at 823 K for 4 h in air flow.
[d] The 7th cycle was performed over the calcined catalyst under the same reaction condition, except for 24 h of reaction time.

in an approximately linear manner with increasing number of Brønsted acid sites of the nanosheets MFI catalyst. The NS-2.5-(48) catalyst displayed the best production of PX among all nanosheets catalysts, as well as among other conventional MFI zeolite catalysts (Table 2). According to the reaction pathway, the Diels-Alder cycloaddition reaction can compete with side reaction routes such as hydrolysis of DMF with water inside the micropores of zeolite catalysts, as shown in Fig. S3 [35]. It is, therefore, important to remove water from the reaction, as well as to control the acidity of the zeolite catalyst. In fact, the NS-2.5-(48) catalyst can easily produce water as well as PX in the DMF-to-PX reaction due to its strong acidity. During the reaction time, the produced water would increase the HDO production through DMF hydrolysis reaction. However, the NS-2.5-(48) catalyst exhibited the smallest yield of HDO (6.0%) at 24 h of reaction time, among nanosheets MFI zeolite catalysts, even which possessed similar surface property such as hydrophilic nature (Table 3). This is because yielded HDO is easily transformed into DMF by reversible hydrolysis, resulting from the rapid production of PX by a large number of Brønsted acid sites in the DFM-to-PX reaction over the NS-2.5-(48) catalyst [15]. Based on this investigation, it is reasonable to conclude that, the nanosheets MFI zeolite with high Al-containing catalyst can be increased PX production yield from the DMF-to-PX reaction.

3.4. Recyclability of nanosheets MFI zeolite catalyst

We investigate the recyclability of the NS-2.5 sample in the DMF-to-PX reaction. For this investigation, the DMF conversion of the fresh NS-2.5 catalyst was firstly measured in the PX production reaction. The DMF conversion of the fresh NS-2.5 catalyst increased linearly up to 74.2% for 8 h. This conversion level was chosen for comparison of the catalytic activity of the fresh and recycled NS-2.5 samples. For the 2nd reaction run, the used NS-2.5 sample was

Table 5
Physicochemical properties of pristine ZSM-5 and mesoporous MFI-type zeolite samples.

Catalyst	Si/Al[a]	S_{BET} ($m^2\ g^{-1}$)[b]	S_{ext} ($m^2\ g^{-1}$)[c]	V_{tot} ($cm^3\ g^{-1}$)[d]	BA_{tot} ($\mu mol\ g^{-1}$)[e]	BA_{ext} ($\mu mol\ g^{-1}$)[f]
Pristine ZSM-5	14	330	50	0.16	1204 (55)[g]	29 (7)
Meso-ZSM-5-3	11	370	100	0.21	1398 (21)	80 (2)
NS-2.5-(48)	48	620	460	0.73	162 (14)	49 (10)

[a] Si/Al molar ratio obtained from ICP-AES elemental analysis.
[b] S_{BET} is the BET surface area obtained from N_2 adsorption in relative pressure range (P/P_0) of 0.05–0.20.
[c] S_{ext} is the external surface area evaluated from the *t*-plot method.
[d] V_{tot} is the total pore volume obtained at $P/P_0 = 0.95$.
[e] BA_{tot} is the concentration of total Brønsted acid sites.
[f] BA_{ext} is concentration of external Brønsted acid sites.
[g] The values in parenthesis indicate the concentration of the strong Brønsted acid sites.

washed with *i*-propyl alcohol and dried at 373 K. The DMF conversion of the dried NS-2.5 catalyst drastically decreased from 74.2% to 29.6% in the 2nd cycle (Table 4). The DMF conversion decrease was due to the presence of organic species, resulting in the blocking the active sites in the used NS-2.5 sample. The amount of organic compound was around 0.18 g per g catalyst in the spent NS-2.5 sample, as measured by TGA analysis. The organic deposit in the spent NS-2.5 sample could be generated in the form of polymeric coke species through side reactions, such as oligomerization of HDO and electrophilic alkylation of cationic intermediates (Fig. S3) [36]. However, these polymeric compounds in the spent NS-2.5 sample can be simply removed by air calcination. The calcined NS-2.5 sample almost completely recovered its original activity in the 3rd cycle (Table 4). The recovered NS-2.5 catalyst showed 97% of its pristine activity even after five times in the reuse cycle. Furthermore, the DMF conversion of the recovered NS-2.5 catalyst was reached 93% after 24 h of reaction time in the 7th cycle. This recyclability of NS-2.5 could be attributed to the highly stable framework of microporous MFI zeolite structure with its unique mesoporosity. Fig. S4 and S5 show the XRD patterns and N_2 sorption isotherms of fresh and used NS-2.5 catalysts. No significant difference was observed between the fresh and used NS-2.5 catalysts. This indicates the preservation of the crystallinity and porosity of NS-2.5 during the catalyst regeneration step. Also, the strong Brønsted acid sites of the NS-2.5 catalyst can be regenerated by air calcination (Table S6).

3.5. Catalytic performance for DMF-to-PX over mesoporous MFI zeolite from commercial ZSM-5 zeolite

As discussed above, the main catalytic factors for the PX production through Diels-Alder cycloaddition and dehydration reaction from DMF and ethylene over MFI zeolite are mesoporosity and highly acidic properties on the exterior surface. To generalize and prove these factors, a series of MFI-type zeolite with mesoporosity were prepared by simple post-treatments of a commercially available ZSM-5 sample. The commercial available ZSM-5 with the highest Al contents was strategically selected to synthesize mesoporous MFI-type zeolite (Meso-ZSM-5); this was done because an MFI-type zeolite with lower Si/Al ratio possess a larger amount of Brønsted acid sites and a better PX production yield compared to those characteristics of MFI-type zeolite with high Si/Al ratio (see Section 3.3). Fig. S6 shows powder XRD patterns of the prepared Meso-ZSM-5 zeolites and the pristine ZSM-5 zeolite. In the low-angle range, the Meso-ZSM-5-NaOH and the pristine ZSM-5 did not show a distinct XRD peak. However, the Meso-ZSM-5 samples synthesized with TMAOH and CTAB exhibited one peak at around $2\theta = 0.9–1.0^\circ$; this peak indicates the existence of mesopores. The high intensity and greater sharpness of the low-angle XRD peak for the Meso-ZSM-5-3 sample reveal that the mesoporosity developed well compared with the case of the Meso-ZSM-5-2 sample. In the wide-angle region, the Bragg reflections for all Meso-ZSM-5 samples were accordance with those of the pristine commercial

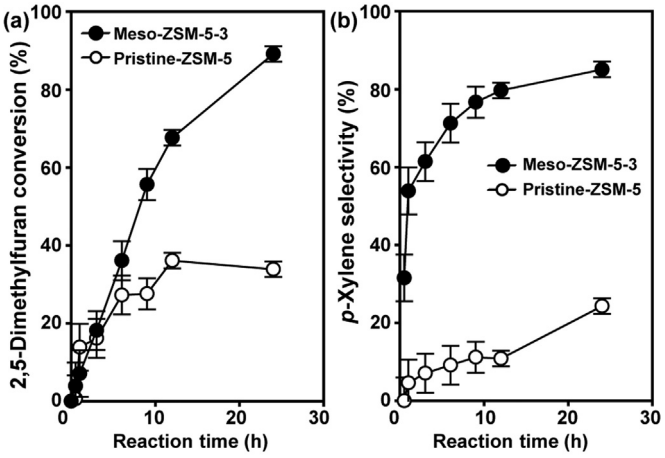

Fig. 7. Conversion of 2,5-dimethylfuran (a) and *p*-xylene selectivity (b) over pristine ZSM-5 and Meso-ZSM-5-3 catalysts as a function of reaction time. Reaction conditions: 0.2 g of catalyst, 25 ml of 2,5-dimethylfuran, 50 bar of ethylene, 75 ml of *n*-heptane (solvent), 523 K.

ZSM-5; however, all Meso-ZSM-5 samples exhibited lower XRD peak intensities compared with that of the pristine ZSM-5 due to a decrease of zeolite crystallinity that stemmed from the formation of mesoporous structure in the pristine ZSM-5 crystals after a post-synthetic treatment.

N_2 sorption isotherms and their corresponding pore size distributions of the pristine ZSM-5 and Meso-ZSM-5 samples were shown in Fig. S7. The isotherms of the Meso-ZSM-5 samples were considerably different from that of the pristine ZSM-5 sample. The isotherm type of Meso-ZSM-5 exhibited types IV isotherms, which is typical of a mesoporous zeolite. The hysteresis loop in the adsorption-desorption isotherm curve was developed, which could indicate the formation of mesoporosity in the pristine ZSM-5 after post-synthetic treatment. The pore size distribution curve more clearly revealed the existence and degree of development mesopores in the prepared mesoporous zeolite samples. The desilicated ZSM-5 sample by NaOH treatment (Meso-ZSM-5-NaOH) possesses both narrow mesopores centered at 4.4 nm and additional mesopores with broad pore size distribution due to the non-selective desilication treatment in NaOH solution. However, the samples treated with a mixture of CTAB and TMAOH (Meso-ZSM-5-2 and Meso-ZSM-5-3) showed relatively narrow one mesopores in the pore size distribution curves. The Meso-ZSM-5-3 showed a sharp distribution of mesopores similar to that of Meso-ZSM-5-2, but the mesopore volume of Meso-ZSM-3 was larger than that of Meso-ZSM-5-2 in the pore size distribution graph. The detailed physicochemical properties of the Meso-ZSM-5 samples are listed in Table S7. The Meso-ZSM-5-3 sample possessed the highest mesoporous properties among the prepared mesoporous MFI-type zeolite from the commercial ZSM-5 zeolite. From these XRD and

Table 6
2,5-Dimethylfuran conversion and product selectivity of pristine ZSM-5 and Meso-ZSM-5-3 catalysts for the DMF-to-PX reaction at 24 h of reaction time.

Catalyst	H-TOF (10^{-3} s^{-1})[a]	DMF Conv (%)	NPA ($\times 10^{-3}$)[b]	PX Yield (%)	Selectivity (%)[c]			
					PX	MX	HDO	Unknown Products
Pristine ZSM-5	0.8	33.9	0.33	8.4	24.3	0.0	13.6	58.7
Meso-ZSM-5-3	4.4	89.1	0.74	75.8	85.1	0.6	0.2	12.1

[a] H-TOF is the turnover frequency calculated by normalizing the rate by the number of Brønsted acid sites at the reaction time = 1 h.
[b] NPA is the number of molecules per acids site is calculated by the mole of reacted DMF by the number of Brønsted acid sites in the catalyst.
[c] MX, *m*-xylene; HDO, 2,5-hexanedione; Unknown products, carbon loss.

N_2 sorption analyses, we concluded that the optimum mesoporous MFI-type zeolite for DMF-to-PX is the Meso-ZSM-5-3 sample, which has well-developed mesoporosity and large surface area and which retained a microporous MFI-zeolitic structure.

The representative electron microscopy images of the Meso-ZSM-5-3 and the pristine ZSM-5 samples are shown in Fig. 6. The pristine ZSM-5 zeolite was composed of clustered primary particles with randomly shaped nanocrystals with particle sizes ranging from 100 to 500 nm. These primary particles exhibited both smooth facets with cracks and broken grains. However, the SEM image of the Meso-ZSM-5-3 sample shows aggregation of slit-shaped crystals after post-treatment of the pristine ZSM-5. The TEM image of the Meso-ZSM-5-3 sample visibly shows the existence of mesopores, while the pristine ZSM-5 displayed a smooth surface in the TEM image. These mesopores were in a random and disordered array in the Meso-ZSM-5-3 sample. This mesoporous structure is in good agreement with the N_2 sorption analysis.

The Si/Al ratio of Meso-ZSM-5-3, compared with the Si/Al ratio of the pristine ZSM-5, was reduced due to the dissolving of a certain amount of silica species during the formation of the mesopores (Table 5). Both BET specific and external surface areas increased with the formation of mesopores in the Meso-ZSM-5-3. Especially, the value of the external surface area was 2-fold higher than that of pristine ZSM-5 samples. The concentration and location of Brønsted acid sites in the pristine ZSM-5 and Meso-ZSM-5-3 samples were also determined by ^{31}P NMR analysis using TMPO and TBPO (Fig. S8). Compared with the pristine ZSM-5 (BA_{tot} = 1204 μmol g^{-1}, BA_{ext} = 29 μmol g^{-1}), the Meso-ZSM-5-3 had a high density of total and external Brønsted acid sites (BA_{tot} = 1398 μmol g^{-1}, BA_{ext} = 80 μmol g^{-1}). This is attributed to the low Si/Al ratio and the high external surface area of the Meso-ZSM-5-3 sample. However, the number of strong Brønsted acid sites on the surface of Meso-ZSM-5-3 (strong BA_{tot} = 21 μmol g^{-1}, BA_{ext} = 2 μmol g^{-1}) was much lower than that of the pristine ZSM-5 (strong BA_{tot} = 55 μmol g^{-1}, BA_{ext} = 7 μmol g^{-1}). The highest chemical shift value of the ^{31}P NMR spectra using TMPO (86 ppm) and TBPO (92 ppm) was the strong Brønsted acid sites, as shown in Fig. S8. Spectra of strong Brønsted acid sites from ^{31}P NMR using both TMPO and TBPO in the pristine ZSM-5 were relatively higher than those in the Meso-ZSM-5-3 sample. If the composition of the Meso-ZSM-5-3 (Si/Al = 11) was similar to that of the pristine ZSM-5 sample (Si/Al = 14), the strong Brønsted acid sites would be converted to weaker Brønsted acid sites. Particularly, ^{31}P NMR spectra of TBPO adsorbed on the Meso-ZSM-5-3, indicated in Fig. S8 (e) clearly showed a decrease of NMR spectra for the strong Brønsted acid sites (92 ppm) and an increase of NMR spectra for the weak Brønsted acid sites (72 ppm) compared with those values for the pristine ZSM-5 after formation of mesopores. The observed result is in good agreement with a recent study [37].

The catalytic activities of the Meso-ZSM-5-3 and the pristine ZSM-5 catalysts were tested in the DMF-to-PX reaction. The reaction condition for these catalysts was the same as that for the nanosheets MFI zeolites discussed in Section 3.2. Fig. 7 shows plots of DMF conversion and PX selectivity over the Meso-ZSM-5-3 and the pristine ZSM-5 catalysts with reaction time. At the initial period, the DMF conversion of the pristine ZSM-5 catalyst was higher than that of the Meso-ZSM-5-3 catalyst, while the DMF selectivity of the Meso-ZSM-5-3 was superior to that of the pristine ZSM-5. These results can be explained by the strong Brønsted acidic properties of internal active sites in the pristine ZSM-5 compared with the case of the Meso-ZSM-5-3. The low PX selectivity of the pristine ZSM-5 catalyst might produce a large amount of by-products (HDO selectivity = 11.7%, unknown products selectivity = 57.6%). Among the by-products, the unknown products were composed of alkylated products and oligomers, as confirmed by GC–MS analysis (Fig. S9). This result is good agreement with previous report [35]. These unknown products would be precursors of coke formation and lead to quick deactivation of the catalyst. After the initial reaction period, DMF conversion and PX selectivity over the pristine ZSM-5 catalyst increased to the maximum conversion value (35.1%) at 12 h, with very low PX selectivity (10.9%). However, the DMF conversion and the PX selectivity over the Meso-ZSM-5-3 catalyst gradually increased until 24 h. As shown in Table 6, the values of DMF conversion and PX selectivity were 89.1% and 85.1% at 24 h, respectively. If the reaction time was over 24 h, the Meso-ZSM-5-3 catalyst should have higher values of DMF conversion and PX selectivity because it was not at its maximum point at 24 h reaction time. Therefore, PX yield of the Meso-ZSM-5 catalyst significantly increased and became over 9 fold higher than that of the pristine ZSM-5 catalyst in PX production at 24 h reaction time. The high PX yield can be attributed to the intercrystalline mesopores in Meso-ZSM-5. The exposed Brønsted acid sites on the exterior surface increased DMF conversion and decreased the formation of by-products, which lead to deactivation of the catalyst in DMF-to-PX reaction.

To allow a comparison of the catalytic activity of the Meso-ZSM-5-3 with those of the other mesoporous zeolite catalysts in the DMF-to-PX reaction using the same reactor system at 24 h, the detailed catalytic results are listed in Table S8 and S9. High DMF conversions of over 95% were shown in two mesoporous zeolites, nano-sponge beta zeolite [NSP-BEA (30)] and NS-2.5-(48), which were synthesized *via* the hydrothermal synthesis route using multi-ammonium surfactant SDAs [16,38]. Due to the highly mesoporous structure with BA_{ext} in the NSP-BEA (30) and NS-2.5-(48) catalysts, the DMF-to-PX reactions over these two mesoporous zeolites were faster, and almost finished at 24 h compared with the Meso-ZSM-5-3 catalyst with relatively less mesoporous structure. In particular, NS-2.5-(48) catalyst exhibited higher initial reaction rates (DMF reaction rate and PX production rate) than Meso-ZSM-5-3 catalyst (Table S9). This result may due to the enhanced molecular diffusion of the NS-2.5 sample with high external surface area and large pore volume. Even though, among the mesoporous zeolites, the Meso-ZSM-5-3 catalyst had a slow reaction rate, it exhibited the highest PX selectivity and the lowest by-products such as HDO and unknown products. These unique catalytic natures in the Meso-ZSM-5-3 catalyst such as the slow reaction rate and high PX selectivity can be explained by the number of strong BA_{ext} (obtained by ^{31}P NMR analyses as shown in Fig. S8 and Table 5). Even at a high Si/Al ratio = 48, the NS-2.5-(48) catalyst exhibited a

large number of strong BA_{ext} (10 μmol g^{-1}) compared with the case of the Meso-ZSM-5-3 catalyst (Si/Al = 11, 2 μmol g^{-1}). The large number of strong BA_{ext} of NS-2.5-(48) could increase the rate of DMF conversion, but this strong BA_{ext} could also increase side-reactions to produce by-products and coke. As discussed above, the pristine ZSM-5 catalyst with a relatively high number of strong BA_{ext} (7 μmol g^{-1}) compared with the Meso-ZSM-5, also showed a high reaction rate of DMF conversion with high selectivity to by-products in the initial reaction period; however, for prolonged times, the absence of mesopores in the pristine ZSM-5 can lead to low reactivity due to fast deactivation by coke formation. From these results, it can be seen that the strong BA_{ext} in mesoporous zeolite catalysts can increase the DMF conversion, but decrease the PX selectivity. However, the PX selectivity can be enhanced by the weak BA_{ext}, which were newly formed by the pseudomorphic synthesis. Therefore, the Meso-ZSM-5-3 synthesized from commercial ZSM-5 can be a comparable catalyst to mesoporous zeolites synthesized with a complex SDA.

4. Conclusion

We investigated the Diels-Alder cycloaddition and dehydration reaction of 2,5-dimethylfuran (DMF) with ethylene over MFI-type zeolites with different crystal thicknesses (2.5–500 nm) and various Si/Al ratios (48–340). The catalytic activity and *p*-xylene (PX) selectivity increased with decreasing zeolite crystal thickness. Among all the investigated catalysts, the nanosheets MFI zeolite catalyst exhibited the highest catalytic performance in PX formation from DMF and ethylene. This result can be accounted for by the many strong Brønsted acid sites located on zeolite exterior surfaces, which result in enhanced molecular diffusion. These external catalytic sites of the nanosheets MFI zeolite may provide unique opportunities for this material to become a promising catalyst for various catalytic applications that involve bulky species. Furthermore, these catalytic factors can be extended to commercially available ZSM-5 zeolite. The mesoporous MFI-type zeolite prepared from commercial ZSM-5 exhibited a superior PX yield to that of pristine ZSM-5, and showed a comparable the catalytic performance to other mesoporous zeolite synthesized with multi-ammonium containing a structure-directing surfactant.

Acknowledgements

The authors would like to acknowledge the funding from the R&D Convergence Program of the MSIP (Ministry of Science, ICT and Future Planning) and NST (National Research Council of Science & Technology) of the Republic of Korea (CRC-14-1-KRICT). This work was also supported by IBS-R004-D1.

Appendix A. Supplementary data

Supplementary data associated with this article can be found, in the online version, at http://dx.doi.org/10.1016/j.apcatb.2017.01.031.

References

[1] T.P. Vispute, H. Zhang, A. Sanna, R. Xiao, G.W. Huber, Renewable chemical commodity feedstocks from integrated catalytic processing of pyrolysis oils, Science 330 (2010) 1222–1227.
[2] Y.-T. Cheng, J. Jae, J. Shi, W. Fan, G.W. Huber, Production of renewable aromatic compounds by catalytic fast pyrolysis of lignocellulosic biomass with bifunctional Ga/ZSM-5 catalysts, Angew. Chem. 124 (2012) 1416–1419.
[3] P. Wantanachaisaeng, K. O'Neil, Capturing opportunities for para-xylene production, UOP LLC, 2007.
[4] W. Partenheimer, Methodology and scope of metal/bromide autoxidation of hydrocarbons, Catal. Today 23 (1995) 69–158.
[5] C.L. Williams, C.-C. Chang, P. Do, N. Nikbin, S. Caratzoulas, D.G. Vlachos, R.F. Lobo, W. Fan, P.J. Dauenhauer, Cycloaddition of biomass-derived furans for catalytic production of renewable p-xylene, ACS Catal. 2 (2012) 935–939.
[6] Y.Y. Fong, A.Z. Abdullah, A.L. Ahmad, S. Bhatia, Development of functionalized zeolite membrane and its potential role as reactor combined separator for para-xylene production from xylene isomers, Chem. Eng. J. 139 (2008) 172–193.
[7] M. Kareem, S. Chand, I. Mishra, Disproportionation of toluene to produce benzene and p-xylene—a review, J. Sci. Ind. Res. 60 (2001) 319–327.
[8] R.D. Chirico, W.V. Steele, Thermodynamic equilibria in xylene isomerization. 5. Xylene isomerization equilibria from thermodynamic studies and reconciliation of calculated and experimental product distributions, J. Chem. Eng. Data 42 (1997) 784–790.
[9] P.C.A. Bruijnincx, B.M. Weckhuysen, Shale gas revolution: an opportunity for the production of biobased chemicals? Angew. Chem. Int. Ed. 52 (2013) 11980–11987.
[10] M.W. Peters, J.D. Taylor, M. Jenni, L.E. Manzer, D.E. Henton, Integrated process to selectively convert renewable isobutanol to p-xylene, US20110087000 A1, 2011.
[11] G.W. Huber, Y.T., Cheng, Z., Wang, W. Fan, Method for converting a hydrocarbonaceous material to a fluid hydrocarbon product comprising p-xylene, US20130324772 A1, 2013.
[12] R.D. Cortright, P.G. Blommel, Synthesis of liquid fuels and chemicals from oxygenated hydrocarbons, US8455705 B2, 2013.
[13] T.A. Brandvold, Carbohydrate route to para-xylene and terephthalic acid, US20100331568 A1, 2010.
[14] T.A. Brandvold, Carbohydrate route to para-xylene and terephthalic acid, US8314267 B2, 2012.
[15] C.-C. Chang, S.K. Green, C.L. Williams, P.J. Dauenhauer, W. Fan, Ultra-selective cycloaddition of dimethylfuran for renewable p-xylene with H-BEA, Green Chem. 16 (2014) 585–588.
[16] T.-W. Kim, S.-Y. Kim, J.-C. Kim, Y. Kim, R. Ryoo, C.-U. Kim, Selective p-xylene production from biomass-derived dimethylfuran and ethylene over zeolite beta nanosponge catalysts, Appl. Catal. B 185 (2016) 100–109.
[17] M. Choi, K. Na, J. Kim, Y. Sakamoto, O. Terasaki, R. Ryoo, Stable single-unit-cell nanosheets of zeolite MFI as active and long-lived catalysts, Nature 461 (2009) 246–249.
[18] K. Na, M. Choi, W. Park, Y. Sakamoto, O. Terasaki, R. Ryoo, Pillared MFI zeolite nanosheets of a single-unit-cell thickness, J. Am. Chem. Soc. 132 (2010) 4169–4177.
[19] W. Park, D. Yu, K. Na, K.E. Jelfs, B. Slater, Y. Sakamoto, R. Ryoo, Hierarchically structure-directing effect of multi-ammonium surfactants for the generation of MFI zeolite nanosheets, Chem. Mater. 23 (2011) 5131–5137.
[20] J. Jung, C. Jo, K. Cho, R. Ryoo, Zeolite nanosheet of a single-pore thickness generated by a zeolite-structure-directing surfactant, J. Mater. Chem. 22 (2012) 4637–4640.
[21] Y. Kim, J.-C. Kim, C. Jo, T.-W. Kim, C.-U. Kim, S.-Y. Jeong, H.-J. Chae, Structural and physicochemical effects of MFI zeolite nanosheets for the selective synthesis of propylene from methanol, Microporous Mesoporous Mater. 222 (2016) 1–8.
[22] J.-C. Kim, K. Cho, S. Lee, R. Ryoo, Mesopore wall-catalyzed Friedel-Crafts acylation of bulky aromatic compounds in MFI zeolite nanosponge, Catal. Today 243 (2015) 103–108.
[23] J. Kim, M. Choi, R. Ryoo, Effect of mesoporosity against the deactivation of MFI zeolite catalyst during the methanol-to-hydrocarbon conversion process, J. Catal. 269 (2010) 219–228.
[24] W. Kim, R. Ryoo, Probing the catalytic function of external acid sites located on the MFI nanosheet for conversion of methanol to hydrocarbons, Catal. Lett. 144 (2014) 1164–1169.
[25] J.-C. Kim, R. Ryoo, M.V. Opanasenko, M.V. Shamzhy, J. Čejka, Mesoporous MFI zeolite nanosponge as a high-performance catalyst in the pechmann condensation reaction, ACS Catal. 5 (2015) 2596–2604.
[26] J.-C. Kim, K. Cho, R. Ryoo, High catalytic performance of surfactant-directed nanocrystalline zeolites for liquid-phase Friedel–Crafts alkylation of benzene due to external surfaces, Appl. Catal. A 470 (2014) 420–426.
[27] Y.-J. Lee, E.S. Kim, T.-W. Kim, C.-U. Kim, K.-E. Jeong, C.-H. Lee, S.-Y. Jeong, Ring opening of naphthenic molecules over metal containing mesoporous Y zeolite catalyst, J. Nanosci. Nanotechnol. 15 (2015) 5334–5337.
[28] Y. Seo, K. Cho, Y. Jung, R. Ryoo, Characterization of the surface acidity of MFI zeolite nanosheets by 31P NMR of adsorbed phosphine oxides and catalytic cracking of decalin, ACS Catal. 3 (2013) 713–720.
[29] Q. Zhao, W.-H. Chen, S.-J. Huang, Y.-C. Wu, H.-K. Lee, S.-B. Liu, Discernment and quantification of internal and external acid sites on zeolites, J. Phys. Chem. B 106 (2002) 4462–4469.
[30] K. Na, W. Park, Y. Seo, R. Ryoo, Disordered assembly of MFI zeolite nanosheets with a large volume of intersheet mesopores, Chem. Mater. 23 (2011) 1273–1279.
[31] Y.S. Tao, H. Kanoh, L. Abrams, K. Kaneko, Mesopore-modified zeolites: preparation, characterization, and applications, Chem. Rev. 106 (2006) 896–910.
[32] M. Kruk, M. Jaroniec, J.H. Kim, R. Ryoo, Characterization of highly ordered MCM-41 silicas using X-ray diffraction and nitrogen adsorption, Langmuir 15 (1999) 5279–5284.
[33] D. Liu, X. Zhang, A. Bhan, M. Tsapatsis, Activity and selectivity differences of external Brønsted acid sites of single-unit-cell thick and conventional MFI and MWW zeolites, Microporous Mesoporous Mater. 200 (2014) 287–290.

[34] N. Nikbin, P.T. Do, S. Caratzoulas, R.F. Lobo, P.J. Dauenhauer, D.G. Vlachos, A DFT study of the acid-catalyzed conversion of 2,5-dimethylfuran and ethylene to p-xylene, J. Catal. 297 (2013) 35–43.
[35] P.T.M. Do, J.R. McAtee, D.A. Watson, R.F. Lobo, Elucidation of Diels-Alder reaction network of 2,5-dimethylfuran and ethylene on HY zeolite catalyst, ACS Catal. 3 (2013) 41–46.
[36] D. Wang, C.M. Osmundsen, E. Taarning, J.A. Dumesic, Selective production of aromatics from alkylfurans over solid acid catalysts, ChemCatChem 5 (2013) 2044–2050.
[37] J. Jung, C. Jo, F.M. Mota, J. Cho, R. Ryoo, Acid catalytic function of mesopore walls generated by MFI zeolite desilication in comparison with external surfaces of MFI zeolite nanosheet, Appl. Catal. A 492 (2015) 68–75.
[38] K. Na, C. Jo, J. Kim, K. Cho, J. Jung, Y. Seo, R.J. Messinger, B.F. Chmelka, R. Ryoo, Directing zeolite structures into hierarchically nanoporous architectures, Science 333 (2011) 328–332.